March 2020

Original Article

Mass Spectrometry Imaging Establishes 2 Distinct Metabolic Phenotypes of Aldosterone-Producing Cell Clusters in Primary Aldosteronism

Na Sun, Lucie S. Meyer, Annette Feuchtinger, Thomas Kunzke, Thomas Knösel, Martin Reincke, Axel Walch, Tracy Ann Williams

Abstract—Aldosterone-producing adenomas (APAs) are one of the main causes of primary aldosteronism and the most prevalent surgically correctable form of hypertension. Aldosterone-producing cell clusters (APCCs) comprise tight nests of zona glomerulosa cells, strongly positive for CYP11B2 (aldosterone synthase) in immunohistochemistry. APCCs have been suggested as possible precursors of APAs because they frequently carry driver mutations for constitutive aldosterone production, and a few adrenal lesions with histopathologic features of both APCCs and APAs have been identified. Our objective was to investigate the metabolic phenotypes of APCCs (n=27) compared with APAs (n=6) using in situ matrix-assisted laser desorption/ionization mass spectrometry imaging of formalin-fixed paraffin-embedded adrenals from patients with unilateral primary aldosteronism. Specific distribution patterns of metabolites were associated with APCCs and classified 2 separate APCC subgroups (subgroups 1 and 2) indistinguishable by CYP11B2 immunohistochemistry. Metabolic profiles of APCCs in subgroup 1 were tightly clustered and distinct from subgroup 2 and APAs. Multiple APCCs from the same adrenal displayed metabolic profiles of the same subgroup. Metabolites of APCC subgroup 2 were highly similar to the APA group and indicated enhanced metabolic pathways favoring cell proliferation compared with APCC subgroup 1. In conclusion, we demonstrate specific subgroups of APCCs with strikingly divergent distribution patterns of metabolites. One subgroup displays a metabolic phenotype convergent with APAs and may represent the progression of APCCs to APAs. **(*Hypertension*. 2020;75:00-00. DOI: 10.1161/HYPERTENSIONAHA.119.14041.)**

● **Online Data Supplement**

Key Words: adenoma ■ adrenal cortex ■ hyperaldosteronism ■ hypertension ■ mass spectrometry

Primary aldosteronism is a common but underdiagnosed cause of secondary hypertension characterized by the overproduction of aldosterone relative to suppressed plasma renin levels.[1,2] Unilateral aldosterone-producing adenomas (APAs) and bilateral adrenal hyperplasia (also called idiopathic hyperaldosteronism) are the main subtypes of primary aldosteronism, which together account for >80% of all diagnosed cases of the disease.[3] Specific monoclonal antibodies to the highly homologous adrenal steroidogenic enzymes CYP11B2 (aldosterone synthase) and CYP11B1 (11β-hydroxylase) have proven valuable for immunohistochemistry studies and have established the broad spectrum of histological abnormality associated with primary aldosteronism.[4,5] In some cases, adrenals from patients with unilateral primary aldosteronism do not show evidence of a well circumscribed APA but display micronodular or diffuse hyperplasia.[4–6] Small nests of CYP11B2-positive cells located beneath the adrenal capsule, referred to as aldosterone-producing cell clusters (APCCs), have been described in normal adrenals and in adrenals from patients with primary aldosteronism.[7–9]

Somatic mutations in genes encoding the ion channels KCNJ5 (or GIRK4 [G protein coupled inwardly rectifying potassium channel]) and CACNA1D (Cav1.3 calcium channel) and the ATP1A1 (Na^+/K^+-ATPase 1) and ATP2B3 (Ca^{2+}-ATPase 3) ion transporters have been identified in APAs, which activate Ca^{2+} signaling in adrenocortical cells and are associated with increased aldosterone production in primary aldosteronism.[10–15] APCCs frequently carry mutations in CACNA1D—a lower incidence is observed in ATP1A1 and ATP2B3, whereas KCNJ5 mutations (highly prevalent in APAs) are largely absent.[6,9] This latter observation is potentially related to the cell toxicity of mutated KCNJ5 and the high expression level of KCNJ5 in APCCs.[16]

Received September 16, 2019; first decision September 30, 2019; revision accepted January 3, 2020.

From the Research Unit Analytical Pathology, German Research Center for Environmental Health, Helmholtz Zentrum München (N.S., A.F., T. Kunzke, A.W.); Medizinische Klinik und Poliklinik IV, Klinikum der Universität München, LMU München, Germany (L.S.M., M.R., T.A.W.); Institute of Pathology, Ludwig-Maximilians-Universität München, Germany (T. Knösel); and Division of Internal Medicine and Hypertension, Department of Medical Sciences, University of Turin, Italy (T.A.W.).

The online-only Data Supplement is available with this article at https://www.ahajournals.org/doi/suppl/10.1161/HYPERTENSIONAHA.119.14041.

Correspondence to Tracy Ann Williams, Medizinische Klinik und Poliklinik IV, Klinikum der Universität München, LMU München, Ziemssenstraße 1, D-80336 München, Germany, Email tracy.williams@med.uni-muenchen.de or Axel Walch, Helmholtz Zentrum München, German Research Center for Environmental Health, Research Unit Analytical Pathology, Ingolstaedter Landstrasse 1, 85764 Neuherberg, Germany, Email axel.walch@helmholtz-muenchen.de

Hypertension **is available at https://www.ahajournals.org/journal/hyp** **DOI: 10.1161/HYPERTENSIONAHA.119.14041**

The origin of APAs is unknown. The identification of APCC mutations in genes also mutated in APAs suggests that APCCs may represent precursors of APAs.[9] This proposal is seemingly supported by the description of a few adrenal lesions with histological features characteristic of both APCCs and APAs, interpreted as APCCs transitioning to APAs (referred to as possible APCC-to-APA transitional lesions).[17]

Matrix-assisted laser desorption/ionization mass spectrometry imaging (MALDI-MSI) acquires molecular images based on the spatially resolved, label-free semiquantitative detection of thousands of different molecules in biological specimens.[18–20] We have developed a protocol for high throughput in situ metabolic profiling from formalin-fixed paraffin-embedded (FFPE) samples using a high mass resolution matrix-assisted laser desorption/ionization Fourier-transform ion cyclotron resonance mass spectrometry imaging (MALDI-FT-ICR-MSI) platform for the detection of over 1700 metabolites within the mass range of m/z 50 to 1000.[21,22] This technique has been recently used in several metabolic profiling studies of endocrine tissues and successfully applied to visualize the distribution of hormones and metabolites in the normal and diseased adrenal.[23–26]

Here, we used in situ metabolic imaging analysis by MALDI-FT-ICR-MSI of FFPE adrenals resected from patients with unilateral primary aldosteronism to investigate the potential existence of diverse metabolic phenotypes of APCCs.

Methods

The data that support the findings of this study are available from the corresponding authors on reasonable request.

Patient Samples

The study was performed on 16 adrenals removed by unilateral adrenalectomy from patients diagnosed with unilateral primary aldosteronism according to the diagnostic flowchart recommended by the Endocrine Society Guideline with an adrenal venous sampling protocol described previously.[27,28] Samples were selected from surgical cases from the Medizinische Klinik IV, Klinikum der Ludwig-Maximilians-Universität München, Munich, Germany, over a 2-year period (n=63). The 16 adrenal samples comprised adrenals with the AQ8 unusual histopathologic phenotype of unilateral PA with the absence of an APA and the presence of APCCs from a consecutive series of 63 adrenals surgically removed in the 2-year period (n=10) and the first 6 operated adrenals of the series with the prevalent histopathologic phenotype of an APA (used as controls). An APCC was defined as a CYP11B2-positive aggregate of cells beneath the adrenal capsule. A flowchart showing the sample set of adrenals and analyses F1 performed is shown in Figure 1. One adrenal (sample 3-4) showed 3 APCCs in the cortical tissue adjacent to the APA, which were also analyzed. In total, 27 APCCs were used for metabolic profiling analyses and compared with CYP11B2-positive regions of 6 APAs. All patients gave informed consent, and the protocol was approved by the local ethics committee.

MALDI-MSI Experiments

FFPE adrenal samples were cut into 3-µm sections on a microtome (HM 355S, Microm; ThermoScientific) and mounted onto indium-tin-oxide–coated glass slides. The FFPE sections were incubated at 60°C for 1 hour, deparaffinized in xylene (2×8 minutes), and dried on a hot plate at 37°C. The matrix solution consisted of 10 mg/mL 9-aminoacridine hydrochloride monohydrate (Sigma-Aldrich, Germany) in water/methanol 30:70 (v/v). SunCollect automatic sprayer (Sunchrom, Friedrichsdorf, Germany) was used for matrix application. The flow rates were 10, 20, 30, and 40 µL/min, respectively, for the first 4 layers. The other 4 layers were performed at 40 µL/min. The MALDI-MSI measurement was performed on a Bruker Solarix 7T FT-ICR-MS (Bruker Daltonik, Bremen, Germany) in negative ion mode using 50 laser shots per spot at a frequency of 1000 Hz. The MALDI-MSI data were acquired over a mass range of m/z 50 to 1000 with 50-µm lateral resolution. After MALDI-MSI measurements, acquired data underwent spectra processing in FlexImaging v. 4.0 (Bruker Daltonics, Bremen, Germany) and SCiLS Lab v. 2019 (Bruker Daltonics). MALDI-MSI data were normalized to the root mean square of all data points.

Immunohistochemistry and Image Analysis

Sequential adrenal sections for MALDI-MSI experiments were used for immunostaining. CYP11B2 immunohistochemistry was performed under standardized conditions on a Discovery XT automated stainer (Ventana Discovery XT Systems, Ventana Medical Systems, Inc, Tucson) using monoclonal antibodies against human CYP11B2 (diluted 1:100, a gift from Prof Celso Gomez-Sanchez, University of Mississippi), and detected by the Discovery DAB Map Kit (Roche Diagnostics/Ventana Medical Systems), including incubation with anti-mouse and anti-rabbit ready-to-use universal secondary antibodies (catalog 760-4205; Roche Diagnostics/Ventana Medical Systems). APCC regions were annotated according to the CYP11B2 immunostaining. The average spectral data of annotated APCC regions were exported from FlexImaging v. 4.0 (Bruker Daltonics) and used for further bioinformatics analysis.

Bioinformatics Analysis and Metabolite Annotation

MATLAB R2014b (v.7.10.0; Mathworks, Inc, Natick, MA) was used for preprocessing of matrix-assisted laser desorption/ionization spectra as described previously.[21,29] Mass spectra underwent resampling, smoothing, and baseline subtraction to decrease the data dimensionality and to remove noise-level peaks and artifacts. Peak picking was performed using an adapted version of the LIMPIC algorithm[30] with m/z 0.0005 minimum peak width. The signal-to-noise and intensity threshold was set to 2 and 0.01%, respectively. Isotopes were automatically identified and excluded. Peaks in the mass range of m/z 50 to 1000 were resolved and annotated by accurate mass matching in Human Metabolome Database (http://www.hmdb.ca/) and METASPACE (http://annotate.metaspace2020.eu/; ion mode: AQ11 negative; adduct type: [M−H], [M−H−H2O], [M+Na−2H], [M+Cl], and [M+K−2H]; mass accuracy, ≤4 ppm).[31,32] Pathway analysis was performed with the MetaboAnalyst 4.0 (http://www.metaboanalyst.ca)[33,34] and Kyoto Encyclopedia of Genes and Genomes database (http://www.genome.jp/kegg/).[35]

For pathway enrichment analysis of CYP11B2-positive regions, the MS spectrum of each individual region (region 1, 2, or 3) was compared with the average spectrum of regions 1, 2, and 3 combined. Masses with a peak intensity higher than the average spectrum were defined as discriminative masses of the corresponding region. The discriminative masses of each region were then annotated in metabolite databases (Human Metabolome Database and METASPACE). Pathway analyses were performed with MetaboAnalyst 4.0. Briefly, algorithms including hypergeometric test for overrepresentation analysis and relative-betweenness centrality for pathway topology analysis were selected. Homo sapiens (Kyoto Encyclopedia of Genes and Genomes) were specified as pathway library. The metabolome view was generated according to the *P* from the pathway enrichment analysis and pathway impact values from the pathway topology analysis.[33,34]

Hierarchical clustering analysis and component analysis by sparse partial least squares discriminant analysis were performed with MetaboAnalyst 4.0.[33] Briefly, peak lists with respective intensities were uploaded, without data filtering or data transformation and without scaling. Using MetaboAnalyst, a heat map was created to visualize sample clustering based on the 182 annotated mass peaks. Each colored cell on the map corresponds to an intensity value, with samples in rows and features in columns. Euclidean distance and Ward method were applied for clustering analysis. The sparse partial least squares discriminant analysis algorithm was used for discriminant analysis with data shown on a 2-dimensional score plot with the *x* axis representing component

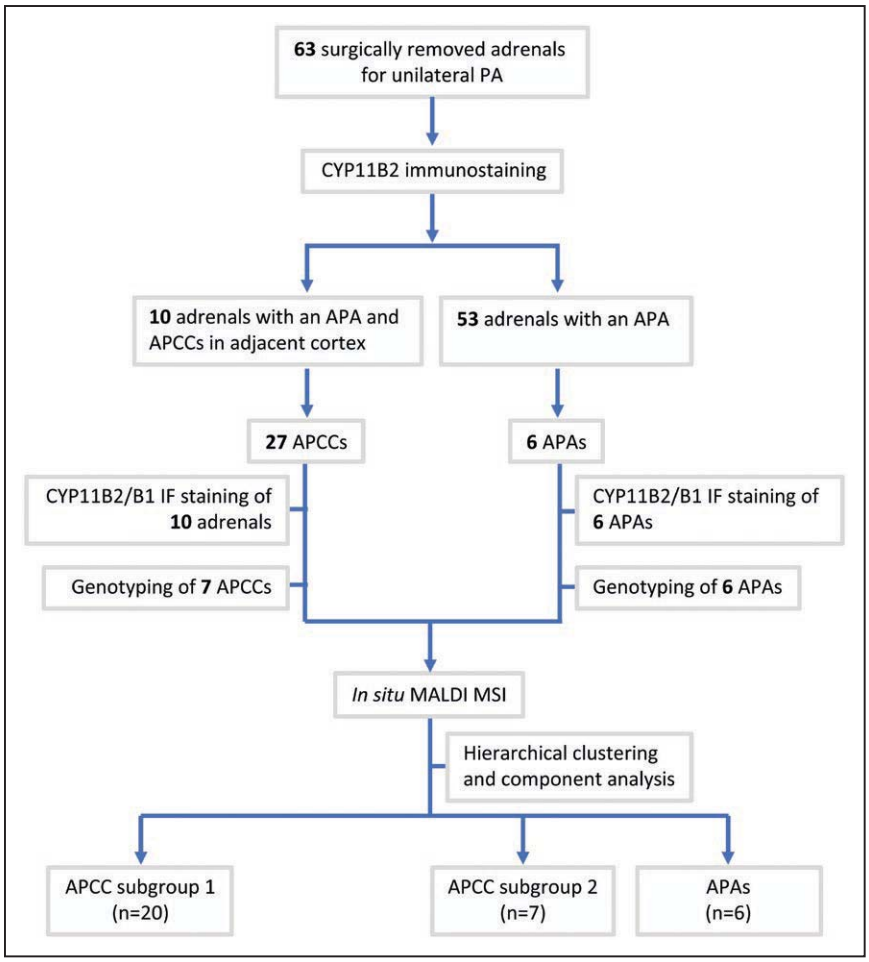

Figure 1. Study workflow for the analysis of surgical adrenal specimens from patients with unilateral primary aldosteronism. Flowchart illustrating the number of adrenals or aldosterone-producing cell clusters (APCCs) used for each analytical step of the study. APA indicates aldosterone-producing adenoma; and MALDI-MSI, matrix-assisted laser desorption/ionization mass spectrometry imaging. AQ9 AQ10

1 and the *y* axis representing component 2. Box plots were created with GraphPad PRISM v. 5.00 (GraphPad Software, Inc, La Jolla). Statistical significance testing was performed using the 1-way ANOVA and Kruskal-Wallis test (α=0.05).

CYP11B2 and CYP11B1 Double Immunofluorescence

Double immunofluorescence CYP11B2 and CYP11B1 staining used monoclonal antibodies against CYP11B2 (clone 41-17B, diluted 1:200) and CYP11B1 (clone 80-7-5, diluted 1:50), both a kind gift from Celso E. Gomez-Sanchez, University of Mississippi. Alexa Fluor 488 anti-mouse and Alexa Fluor 594 anti-rat secondary antibodies both diluted 1:200 were used to detect bound CYP11B2 and CYP11B1 primary antibodies, respectively (Invitrogen). Tissue sections were washed for 7 minutes in 10 mmol/L Copper Sulfate buffer (pH 5) to reduce autofluorescence before mounting with Hard Set mounting medium with DAPI (Vectashield).

Genotyping of FFPE Adrenal Samples

After CYP11B2 immunohistochemistry and metabolic profiling analyses, 7 additional sequential sections of FFPE adrenals were cut for CYP11B2 immunohistochemistry and DNA extraction. The first and last of the 7 additional sections (3 µm, sections 1 and 7) were used for CYP11B2 immunohistochemistry. The intervening sections (10 µm, sections 2–6) were used for DNA extraction of regions corresponding to CYP11B2-positive zones, which were scraped using a 22G Microlance 3 under a stereo microscope. DNA extraction was performed using a Maxwell 16 device according to the manufacturer's protocol. DNA fragments of target sequences were amplified by 35 polymerase chain reaction cycles (annealing temperature, 56–60°C) using around 25 ng template DNA. Polymerase chain reaction products were reamplified by an additional 35 cycles before analysis for specific fragment amplification on a 1% agarose gel, purification (Qiagen QIAquick PCR Purification Kit) and Sanger sequencing. Validation of detected mutations was performed by an independent polymerase chain reaction amplification and Sanger sequencing. Genomic DNA was analyzed for mutations in *KCNJ5*, *ATP1A1* exons 4 and 8, *ATP2B3* exon 8, and *CACNA1D* exons 6, 14, 16, 23, 27, and 32 using primers detailed previously.[36] AQ12

Results

Patient Characteristics and Adrenal Samples

Adrenals were classified into 3 groups stratified by metabolic phenotype: those with APCCs in subgroup 1 (labeled 1-1 to 1-6), APCCs in subgroup 2 (2-1 to 2-4) and group 3 comprising APAs (3-1 to 3-6). The clinical description of the 16 adrenalectomized patients according to subgroup of metabolite clustering (APCC subgroup 1 or 2 or APA) is shown in the Table. Clinical parameters for individual patients and available genotype data are shown in Table S1 in the online-only Data Supplement. In this small group of patients, overall group differences were observed for age and ARR_DRC (P=0.026 and P=0.028, respectively). Pairwise comparisons demonstrated the younger age of APCC subgroup 1 compared with subgroup 2 (P=0.037) and the lower aldosterone-to-renin ratio of APCC subgroup 1 than the APA group (P=0.023). T1

Comprehensive In Situ Metabolic Profiling Analysis Using High-Resolution MALDI-FT-ICR-MSI

APCCs (n=27 from 10 different pieces of adrenal tissue) and regions of 6 different APAs were analyzed using in

Table. Clinical Characteristics of Patients With Unilateral PA According to Metabolic Profiles of Different Groups of Adrenals

Sample ID	APCC Subgroup 1 (n=6)	APCC Subgroup 2 (n=4)	APA (n=6)	Overall *P* Value
Age, y	47±6.7	61±7.6	48±9.1	0.026*
Sex (M/F)	4/2	1/4	1/5	0.115
BMI, kg/m^2	27.7±4.9	28.0±4.4	25.1±5.2	0.566
Duration HTN, mo	71 (39–105)	126 (48–168)	89 (30–156)	0.464
Aldo, pmol/L	333 (300–524)	291 (160–430)	364 (334–954)	0.441
Aldo, ng/dL	12.0 (10.8–18.9)†	10.5 (5.8–15.5)†	12.1 (12.0–34.4)†	0.441
DRC, mU/L	9.5 (3.7–16.4)	2.0 (2.0–4.8)	2.0 (2.0–5.1)	0.059
ARR_DRC	35 (30–128)	91 (74–166)	182 (140–284)	0.028‡
Serum K$^+$, mmol/L	3.1±0.4	3.3±0.5	3.1±0.4	0.617
SBP, mm Hg	145±7.3	155±9.1	146±13.0	0.318
DBP, mm Hg	91±11.0	94±13.8	90±13.6	0.896
Anti-HTN meds (DDD)	1.50 (0.75–4.08)	2.0 (0.3–3.75)	3.0 (0.7–4.4)	0.892

Metabolic profiling separated adrenals into 3 distinct groups based on patterns of metabolites corresponding to APCC subgroups 1 and 2 and APAs. Clinical data of patients in each subgroup are presented as average values ±SD, absolute numbers, or as medians with lower and upper quartiles in parentheses. Numbers of patients in each group are indicated (n). *P* values designate the presence of group differences by the ANOVA and Bonferroni post hoc tests (age, BMI, SBP, and DBP), Kruskal-Wallis test (PAC, DRC, ARR_DRC, and potassium), or χ^2 test (sex). The clinical variables for each individual patient and available genotype data are shown in Table S1. Defined daily dose is the assumed average maintenance dose per day for a drug used from its main indication in adults according to ATC/DDD Index 2018 (https://www.whocc.no/atc_ddd_index/) and can be calculated using an online tool (https://github.com/ABurrello/PASO-Predictor/raw/master/00 - PASO Predictor.xlsm).[45] Aldo indicates plasma aldosterone concentration; APA, aldosterone-producing adenoma; APCC, aldosterone-producing cell cluster; ARR_DRC, aldosterone-to-renin ratio calculated using direct renin concentrations; BMI, body mass index; DBP, diastolic blood pressure; DDD, defined daily dose; DRC, direct renin concentration; F, female; HTN, hypertension; ID, identification; M, male; SBP, systolic blood pressure; and serum K$^+$, lowest serum potassium ion concentration.

*Pairwise difference (*P*=0.037) APCC subgroup 1 vs APCC subgroup 2.

†xxx.

‡Pairwise difference (*P*=0.023) ARR_DRC APCC subgroup 1 vs APA.

situ metabolic mass spectrometry imaging (MSI). The MSI spectra data of >1 million pixels were extracted and subjected to bioinformatics analysis. Within the mass range of m/z 50 to 1000, 182 mass peaks were annotated using the Human Metabolome Database and METASPACE (Table S2). The annotated metabolites covered 46 Kyoto Encyclopedia of Genes and Genomes metabolic pathways. The top 5 most dominant metabolic pathways were amino acid biosynthesis, pentose phosphate pathway, 2-oxocarboxylic acid metabolism, fructose and mannose metabolism, amino sugar, and nucleotide sugar metabolism.

Coregistration of Immunohistochemistry and MALDI-FT-ICR-MSI

An example of the CYP11B2 immunohistochemistry-guided MSI approach is shown for adrenal 1-1 in Figure 2. CYP11B2 immunohistochemistry and spatial distribution of metabolites identified 2 specific patterns of metabolites related to CYP11B2-positive lesions, which are shown for adrenal 1-1 (Figure 2). Pattern 1 displayed a continuous distribution throughout the zona glomerulosa but with absent or low abundance in CYP11B2-positive lesions and was characterized by the localization of *N*-acetylglucosamine sulfate (Figure 2, shown in red). Pattern 2, with GDP as a characteristic metabolite, was highly abundant in APCC regions and had a distribution pattern closely related to CYP11B2 immunostaining but was otherwise largely absent throughout the zona glomerulosa layer (Figure 2, shown in green). The mass peaks that colocalized with the distinct distribution patterns 1 and 2 were automatically elucidated using SCiLS Lab v. 2019 using Pearson correlation analysis. *N*-acetylglucosamine sulfate, belonging to the glycosaminoglycan degradation metabolite pathway, was the only metabolite colocalized with pattern 1, whereas 16 mass peaks colocalized with pattern 2, with biological functions related to purine metabolism and amino acid biosynthesis. The list of the 16 mass peaks colocalized with GDP distribution pattern 2 are shown in Table S3 together with correlation scores for colocalization of each mass peak with GDP.

Figure 2 shows magnified CYP11B2-positive zones (regions 1–3) of adrenal 1-1 (corresponding to regions of interest [ROI] ROI01, ROI02, and ROI03 in Figure 3). Regions 1 and 3 represent high abundance of GDP and an absence of *N*-acetylglucosamine sulfate. Region 2 shows uniform expression of GDP and *N*-acetylglucosamine sulfate without specific localization to the zona glomerulosa. Pathway enrichment analysis identified which metabolite pathways were overrepresented in CYP11B2-positive regions 1 to 3 (Figure 3). Each discriminative pathway associated with regions 1 to 3 is shown in Table S4 with pathway impact and the significance of overall metabolic changes within each pathway.

Metabolic Phenotyping of APCCs

Metabolic data of 27 APCCs and the 6 APA regions were exported and used for hierarchical clustering and component analyses (Figure 4A and 4B, respectively). The hierarchical

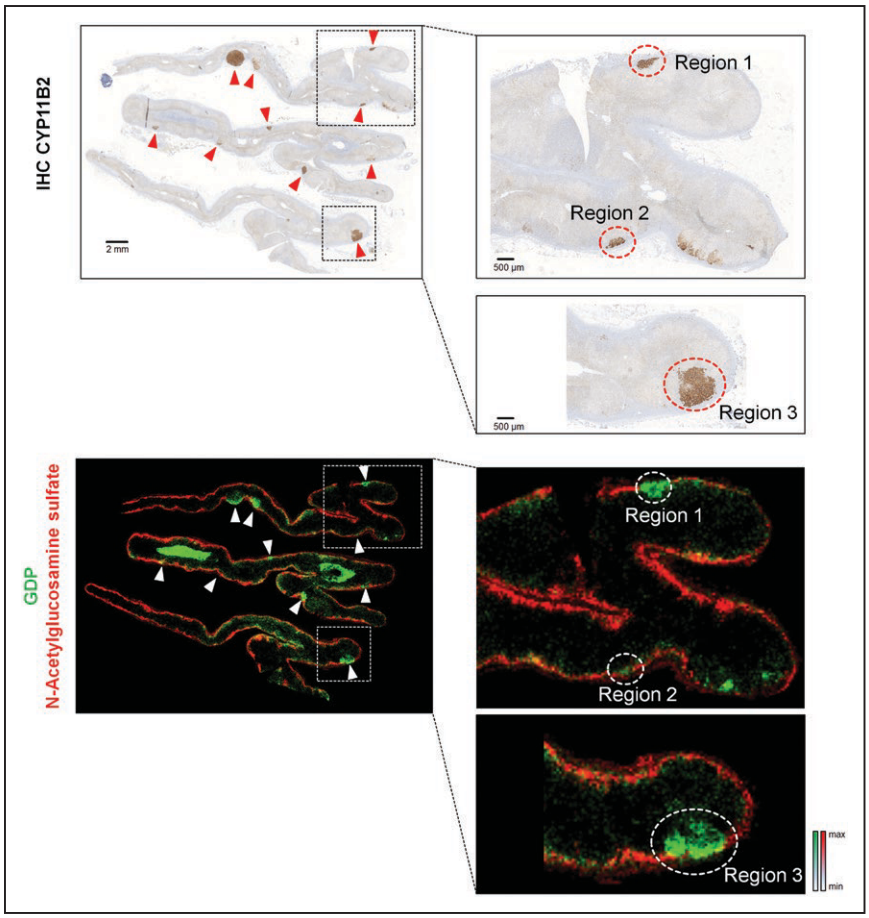

Figure 2. CYP11B2 (aldosterone synthase) immunohistochemistry-guided in situ mass spectrometry imaging of an adrenal showing multiple CYP11B2-positive regions. The figure shows coregistration of *N*-acetylglucosamine sulfate (red) and GDP (GDP, green) with immunohistochemistry of CYP11B2 (aldosterone synthase). Mass spectrometry images and zoomed regions 1, 2, and 3 (regions of interest [ROI]: ROI01, ROI02, and ROI03) of adrenal 1-1 are shown. Red arrows (**top**) indicate CYP11B2-positive regions including aldosterone-producing cell clusters; white arrows (**bottom**) indicate corresponding regions with coregistration of *N*-acetylglucosamine sulfate and GDP. The mass (m/z ratio) of metabolites colocalized with GDP metabolite distribution (pattern 2, see text for details) is shown in Table S3. max indicates maximum; and min, minimum. AQ17

cluster analysis identified groups of adrenals based on the similarity of metabolite patterns. The associated heat map demonstrated a striking separation of APCCs into 2 distinct subgroups (APCC subgroups 1 and 2) with 1 subgroup (subgroup 2) displaying similar metabolite profiles to APAs (Figure 4A). Component analysis using sparse partial least squares discriminant analysis was used to emphasize variations in the metabolite dataset for pattern identification and visualization. APCC subgroup 1, APCC subgroup 2 and APAs were clearly separated with APCCs in subgroup 1 tightly clustered and distinct from APCC subgroup 2 and the APA group. As in the hierarchical cluster analysis, APCC subgroup 2 showed high similarity to the APA group (Figure 4B).

There were no discernable differences at histopathology in APCCs belonging to subgroups 1 and 2 (Figure 4C) or with double immunofluorescence staining for CYP11B2 and CYP11B1 (Figure 4D). In sections analyzed, the APCCs appeared to cover a range of different sizes with a large APCC both in subgroup 1 (adrenal 1-2) and in subgroup 2 (adrenal 2-3).

APCCs originating from the same adrenal displayed similar metabolic profiles. Despite differences in metabolite pathway enrichment (based on discriminative metabolites only) of the 2 APCCs corresponding to regions 1 and 2 of adrenal 1-1 (Figures 2 and 3), hierarchical clustering and component analysis (based on 182 annotated mass peaks) demonstrated their highly similar metabolic profiles classifying both to APCC subgroup 1. Similarly, all 3 APCCs analyzed from adrenal samples 1-1, 1-6, and 3-4 and the 5 APCCs from 1-2 and 4 APCCs from 1-4 were assigned to APCC subgroup 1; the 2 APCCs from adrenal 2-1 and all 3 APCCs from adrenal 2-3 were assigned to APCC subgroup 2 (Figure 4).

The genotypes of the APAs were No Mutation Detected (NMD, 3-1 and 3-5), KCNJ5-Gly151Arg (3-2), KCNJ5-Thr158Ala (3-3), KCNJ5-Leu168Arg (3-4), and ATP1A1-Leu104Arg (3-6). Because of limited tissue availability for APCC samples after metabolic MSI analysis, only a subset of APCCs were genotyped. Available genotypes in APCC subgroup 1: ATP1A1-Gly99Arg (corresponding to ROI03 in adrenal 1-1; a double CACNA1D-Met1344Thr, ATP1A1-Ala114Val mutation [ROI01; Figure S1] and CACNA1D-Ile1342Met [ROI05] in adrenal 1-2; NMD [ROI01] in adrenal 1-3; CACNA1D-Tyr1349His [ROI01] in adrenal 1-4; NMD [ROI01] in adrenal 3-4 [an APCC in the cortical tissue adjacent to the APA in adrenal 3-4]) and in APCC subgroup 2: NMD ([ROI01] in adrenal 2-1; ATP2B3-Val424Ala [ROI01] in adrenal 2-2). The genotyped APCCs are highlighted in Figure 4C and indicated in Table S1. Mutations in KCNJ5 were not detected in any APCC. AQ18

Metabolic Pathway Analysis

Enriched metabolic pathways in APCC or APA subgroups contributing to group discrimination include glycolysis, pentose phosphate pathway, tryptophan metabolism, steroid hormone biosynthesis, purine metabolism, citric acid cycle, amino sugar, and nucleotide sugar metabolism (Figure 5). Specifically, hexose phosphate from glycolysis metabolism, ribose phosphate, and erythrose phosphate from the pentose F5

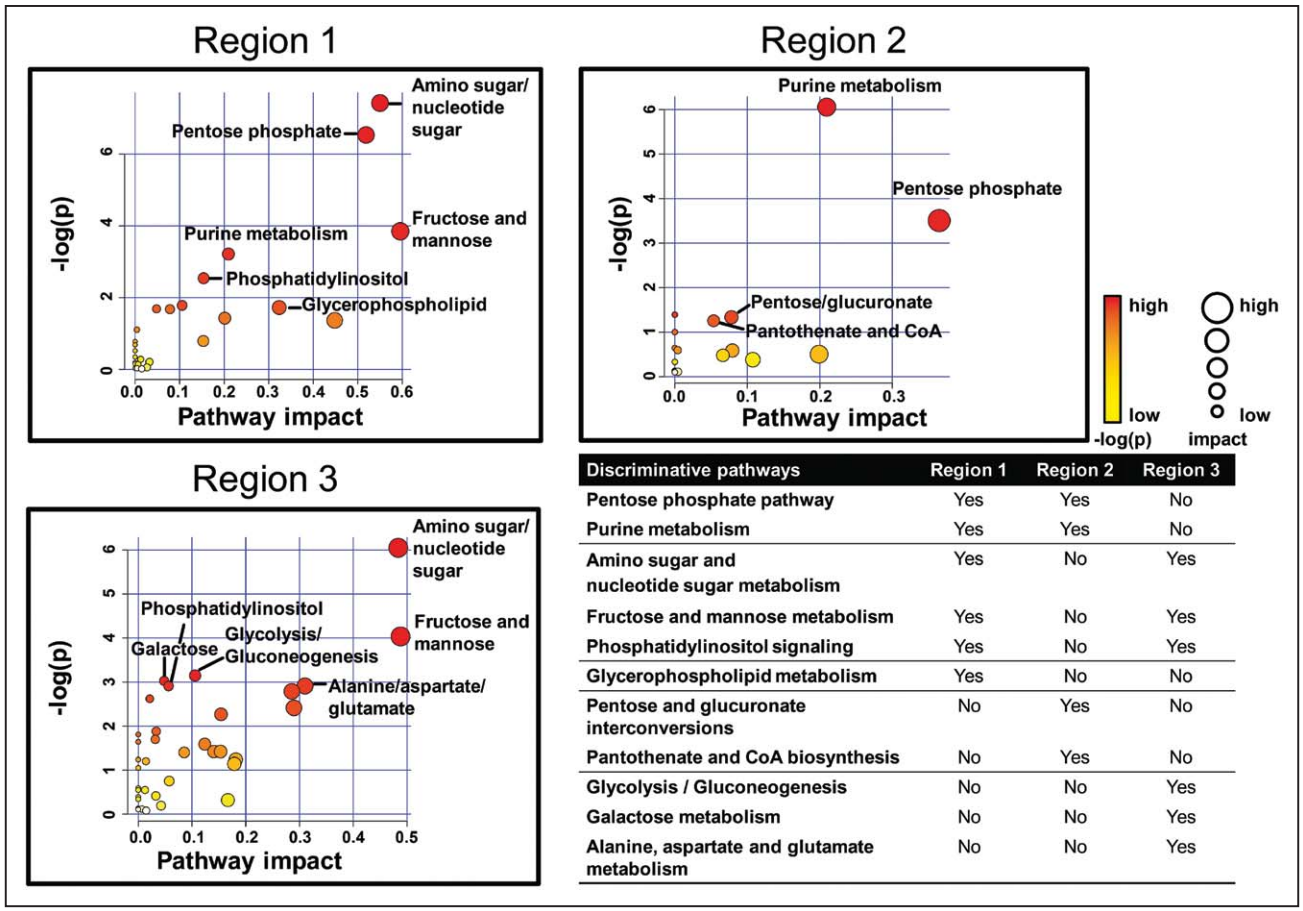

Discriminative pathways	Region 1	Region 2	Region 3
Pentose phosphate pathway	Yes	Yes	No
Purine metabolism	Yes	Yes	No
Amino sugar and nucleotide sugar metabolism	Yes	No	Yes
Fructose and mannose metabolism	Yes	No	Yes
Phosphatidylinositol signaling	Yes	No	Yes
Glycerophospholipid metabolism	Yes	No	No
Pentose and glucuronate interconversions	No	Yes	No
Pantothenate and CoA biosynthesis	No	Yes	No
Glycolysis / Gluconeogenesis	No	No	Yes
Galactose metabolism	No	No	Yes
Alanine, aspartate and glutamate metabolism	No	No	Yes

Figure 3. Pathway enrichment analysis of CYP11B2 (aldosterone synthase)-positive region with distinct metabolic profiles. Pathway enrichment analysis was performed on regions 1, 2, and 3 using MetaboAnalyst 4.0 (http://www.metaboanalyst.ca). Metabolic pathways are represented as circles according to their scores from enrichment (vertical axis) and topology analyses (pathway impact, horizontal axis). The color of circles indicates the statistical significance of the overall metabolic changes within the pathway, and circle diameter represents the relative impact of differential metabolites within the pathway as indicated. The different pattern of discriminative pathways between regions 1 and 3 is summarized in the Table and discriminative pathways associated with each region with pathway impact and significance is shown in Table S4.

phosphate pathway were increased in APCC subgroup 2 and in APAs compared with APCC subgroup 1. In addition, APCC subgroup 2 displayed enhanced metabolism of tryptophan and purine metabolism via the kynurenine pathway, nucleotide derivatives (ADP, GMP, and GDP), and phosphoribosyl glycinamide. The significant enhancement of estrone 3-sulfate and estradiol-17 beta 3-sulfate from steroid hormone biosynthesis, succinate from citric acid cycle and *N*-acetylglucosamine sulfate from amino sugar, and nucleotide sugar metabolism were also observed in APCC subgroup 2.

Discussion

APCCs are characterized by strong and homogeneous CYP11B2 immunostaining and frequently carry variants in genes mutated in APAs, which stimulate CYP11B2 expression and aldosterone overproduction.[9] Nishimoto et al[17] proposed that some APCCs may represent precursors for APAs based on observations of a few cases of CYP11B2-positive micronodular lesions beneath the adrenal capsule comprising both subcapsular APCC-like and inner APA-like components termed pAATLs (possible APCC-to-APA transitional lesions).

AQ20

Metabolic phenotyping combining CYP11B2 immunohistochemistry with in situ MALDI-MSI has been applied recently to the study of the human adrenal. In a metabolic tissue imaging study of normal human adrenals, Sun et al[23] detected a wide range of metabolites, including steroid hormone sulfated metabolites, and established a complex molecular pattern of adrenal zonation.[23] MSI analysis of APCCs is technically challenging because of their small size, but the use of fresh-frozen surgical adrenal specimens enabled visualization of selected steroids with chemical derivatization using Girard T reagent to increase ionization efficiency.[37] Using this approach, Sugiura et al[37] directly detected aldosterone on adrenal samples and demonstrated the coaccumulation of aldosterone and the hybrid steroid 18-oxocortisol, in APCCs and APAs.

Herein, we used immunohistochemistry-guided high spatial resolution MSI for the metabolic visualization of 27 APCCs compared with regions of 6 APAs from archival FFPE adrenal samples.[21,22] The validity of the MSI protocol we used for FFPE tissues was demonstrated by a multicenter interlaboratory round robin study, which showed a high level of between-center reproducibility of FFPE tissue metabolite data.[38] Although removal of hydrophobic lipids during the organic solvent preparation process of FFPE samples was observed, comparison of fresh-frozen and FFPE tissue

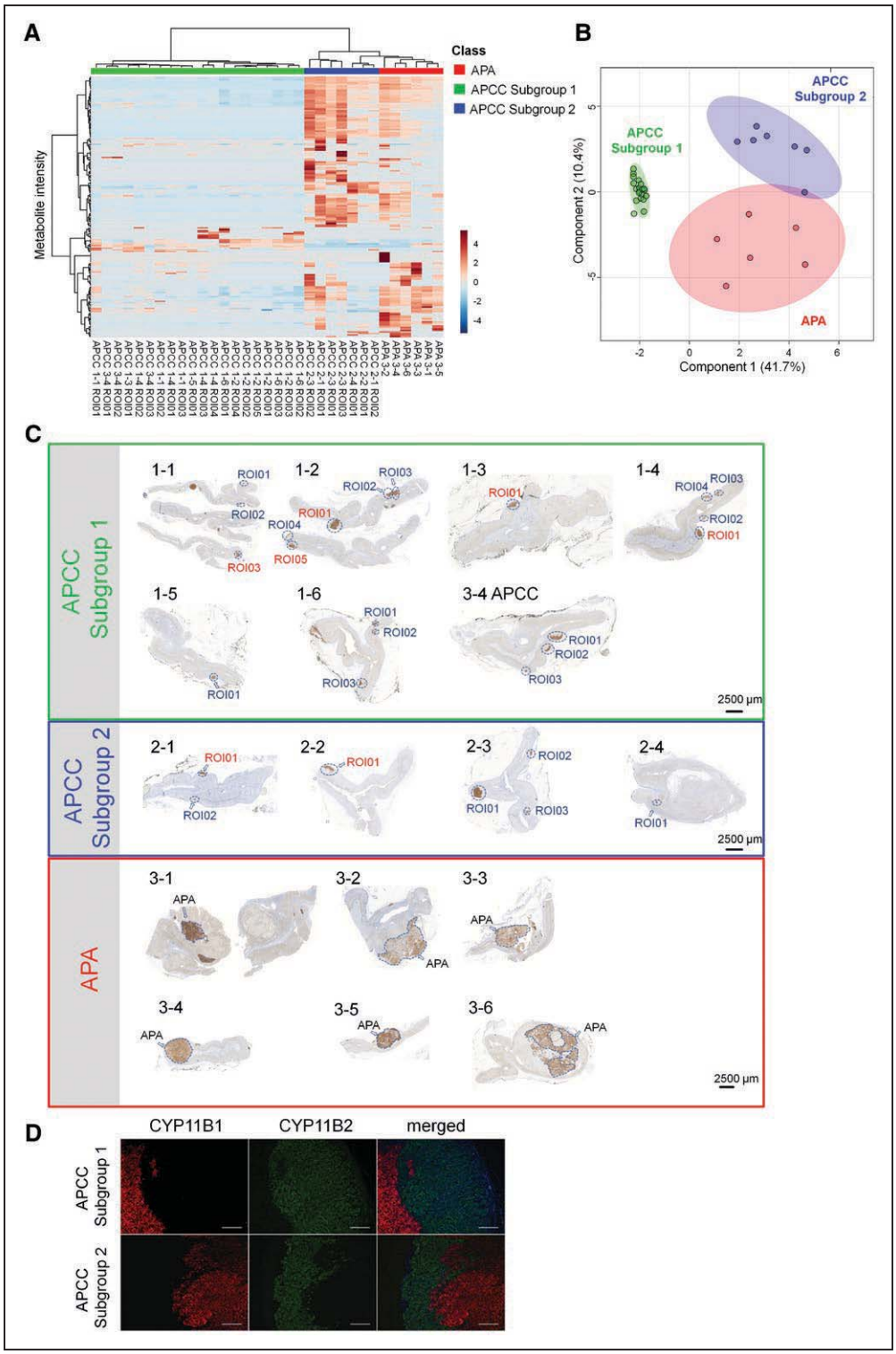

Figure 4. Hierarchical clustering and component analysis. Heat map–based clustering analysis of the 182 mass peaks with a Human Metabolome Database annotation demonstrated different metabolic profiles in aldosterone-producing cell cluster (APCC) subgroup 1, APCC subgroup 2, and aldosterone-producing adenomas (APAs). Peak lists with respective intensities were uploaded to MetaboAnalyst. Each colored cell corresponds to an intensity value, with samples in rows and features in columns. Euclidean distance and Ward method were applied for cluster analysis (**A**). Component analysis using sparse partial least squares discriminant analysis identified 3 patterns of metabolites comprising 2 subgroups of clearly separated APCCs (subgroups 1 and 2) and the APA group (**B**). CYP11B2 (aldosterone synthase) immunohistochemistry of adrenal samples included in the metabolic analyses showing APCCs in subgroup 1, APCCs in subgroup 2, and APAs. Regions of interest (ROI) identification numbers are shown for each APCC analyzed. The ROI identification numbers of genotyped APCCs are indicated in red and are defined in Table S1 (**C**). The metabolic signatures of 3 APCCs in the adrenal cortex adjacent to APA 3 to 4 were analyzed in addition to that of the tumor itself. Double immunofluorescence staining of CYP11B1 (11β-hydroxylase; red) and CYP11B2 (green) of representative APCCs from subgroups 1 and 2 as shown (adrenal 1-4, APCC ROI01; adrenal 2-2, APCC ROI01, respectively; **D**). The merged image also includes DAPI staining in blue. Scale bar=200 µm.

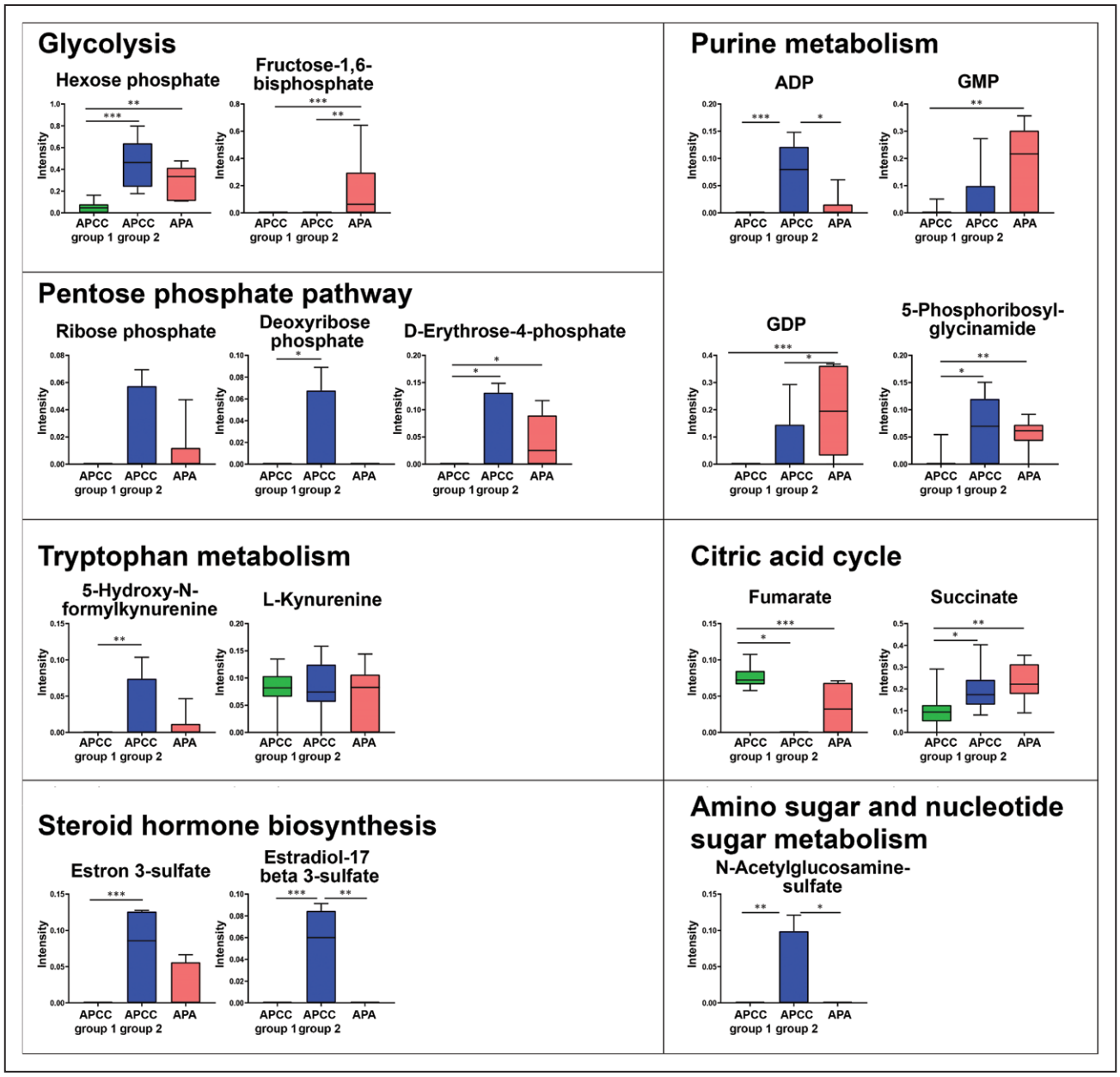

Figure 5. Metabolic pathways distinguish aldosterone-producing cell cluster (APCC) subgroups 1 and 2 and aldosterone-producing adenoma (APA). Box plots of representative metabolites associated with metabolic pathways distinguishing the diverse subgroups of APCCs are shown. One-way ANOVA and Kruskal-Wallis test (α=0.05) were used for statistical analyses (*P<0.05, **P<0.01, ***P<0.001). AQ19

samples revealed a high overlap of metabolic content in the low mass range (Mw 50–400 Da).[21,22] Nevertheless, previous studies have demonstrated that certain steroids can be detected in FFPE tissue.[24,25] Aldosterone was not detected in our study because it requires specific chemical derivatization of fresh-frozen tissue samples.[37]

In contrast to the study of Sugiura et al,[37] our analysis covered a wide range of central metabolic and steroid hormone biosynthesis pathways and determined heterogeneous patterns of metabolites associated with APCCs. Two distinct subgroups of APCCs with markedly divergent metabolic profiles were established. One subgroup (APCC subgroup 1) comprised the majority of the APCCs analyzed (20 of 27 lesions) with tightly clustered patterns of metabolites clearly diverse from the APA group. Conversely, the second subgroup, which included the remaining 7 APCCs, displayed metabolic profiles similar to the APA group (APCC subgroup 2).

APCC subgroup 2 shows evidence of a metabolic switch toward pathways supporting cell proliferation. Hexose monophosphate shunt activity (the pentose phosphate pathway) was increased in APCC subgroup 2 and APAs compared with APCC subgroup 1. This pathway bypasses glycolysis for glucose metabolism and occurs predominantly in tissues synthesizing steroids or fatty acids (such as the adrenal gland and the liver) and supports cell proliferation.[39] Both oxidative and nonoxidative phases of the hexose monophosphate shunt were increased in APCC subgroup 2 as shown by increased ribose phosphate and erythose phosphate, respectively. APCC

subgroup 2 also displays enhanced metabolism of tryptophan via the kynurenine pathway to increase NAD^+ (oxidized nicotinamide adenine dinucleotide) production compared with APCC subgroup 1, which may influence the activity of senescent cells to promote tumor progression.[40]

We also observed a distribution pattern of *N*-acetylglucosamine sulfate remarkably related to CYP11B2-positive lesions. *N*-acetylglucosamine sulfate is a native extracellular glycane fragment and substrate of glycosaminoglycan metabolism. Immunodetection of the glycoproteins laminin and fibronectin in the adult rat adrenal cortex indicates high abundancy in the main ECM (extracellular matrix) of the zona glomerulosa. ECM proteins favor basal proliferation and modulate the effect of hormones.[41] Previous proteomic analyses of APAs reveal an altered ECM composition affecting ECM-cell surface interactions and actin cytoskeleton rearrangements.[42] The low abundance of *N*-acetylglucosamine sulfate in APCC subgroup 1 and the significant enhancement of *N*-acetylglucosamine sulfate in APCC subgroup 2 suggests an altered ECM composition in APCCs, which may be relevant to proliferation and APCC to APA transition.

In a previous in situ MALDI-MSI metabolomics study of a tissue microarray representing 132 genotyped APAs, Murakami et al[25] demonstrated an absence of sample clustering according to genotype in the total dataset. When hierarchical cluster analysis was restricted to genotype pairs, the metabolic profiles of APAs with KCNJ5 mutations could be distinguished from those with CACNA1D mutations. Differences in metabolic signatures between APAs of other genotypes were not detected. Metabolites of purine metabolism and steroidogenesis contributed to this distinction; increased purine synthesis in APAs with KCNJ5 mutations potentially resulted from enhanced cell cycling and proliferation. Herein, metabolites of purine metabolism and steroid hormone biosynthesis were also significant components of the molecular signature, which distinguished APCC subgroups 1 and 2.

In the present study, insufficient sample material for the analysis of both metabolites and genotype only allowed genotype determination for *KCNJ5*, *CACNA1D*, *ATP1A1*, and *ATP2B3* in a subset of APCCs. Notwithstanding this limitation, we demonstrated apparent heterogeneity of genotype in APCC subgroup 1 (NMD, CACNA1D, and ATP1A1 mutations), the absence of KCNJ5 mutations in all APCCs, and an APCC with an ATP2B3 mutation in subgroup 2. Because only a pairwise comparison of APAs with KCNJ5 and CACNA1D mutations resulted in sample clustering in the MALDI-MSI metabolomics study of Murakami et al,[25] it is unlikely that differences in genotype determined the discrimination of APCCs in subgroups 1 and 2.

Both subgroups of APCCs comprise lesions of a range of different sizes, and there was no evident differentiation of the 2 diverse metabolic subgroups based on histopathology. In all 7 adrenals with multiple APCCs, those originating from the same adrenal display similar metabolic profiles and classify to the same subgroup. Patient-related intra-adrenal or circulating factors specific to subgroup 2 may contribute to and at least partially explain this finding. We recently demonstrated that agonistic AT1R-Ab (angiotensin II receptor type 1 autoantibody) levels were higher in patients with primary aldosteronism with evidence of adrenal hyperplasia at computed tomography scanning than those without hyperplasia.[43,44] In the present context, chronic stimulation of the zona glomerulosa cells of APCCs by agonistic AT1R-Abs in a subset of patients with primary aldosteronism may lead to cell proliferation and nodule formation.

In conclusion, we present the first high throughput in situ metabolic MSI analysis of FFPE adrenal tissue samples from patients with primary aldosteronism using a high mass resolution MALDI-FT-ICR-MSI platform. We establish heterogeneous metabolic profiles of APCCs, which determine 2 specific subgroups. The diverse APCC subgroups are, in part, characterized by the differential activation of metabolic pathways leading to cell proliferation and tumorigenesis, which may favor the progression of a subset of APCCs toward the molecular phenotype of APAs.

Perspectives

We will apply the MALDI-FT-ICR-MSI platform we have developed for the analysis of archival FFPE adrenal tissues to provide further insight into the role of APCCs in primary aldosteronism as well as addressing the complex histopathologic phenotypes of this disease.

Since the correlation between APCCs and steroid production is still poorly understood, it will be necessary to perform in situ chemical derivatization with MALDI-MSI using fresh-frozen tissue samples (both normal adrenals and surgical adrenal specimens from patients with primary aldosteronism) for the detection of steroids and any biased colocalization to specific APCC subgroups.

Acknowledgments

We thank Claudia-Marieke Pflüger, Ulrike Buchholz, Cristina Huebner Freitas, Elenore Samson, and Andreas Voss from the Research Unit Analytical Pathology for providing technical assistance. AQ21

Sources of Funding

This work was supported by the European Research Council under the European Union Horizon 2020 research and innovation programme (grant agreement No. 694913 to M. Reincke), the Deutsche Krebshilfe (No. 70112617 to A. Walch), and by the Deutsche Forschungsgemeinschaft (DFG; German Research Foundation) Projektnummer: 314061271-TRR 205 to M. Reincke, A. Walch, and T.A. Williams, and by DFG grant RE 752/20-1 to M. Reincke. This work was also supported by the Else Kröner-Fresenius Stiftung in support of the German Conns Registry-Else-Kröner Hyperaldosteronism Registry (2013_A182 and 2015_A171 to M. Reincke).

Disclosures

None.

References

1. Stowasser M, Gordon RD. Primary aldosteronism: changing definitions and new concepts of physiology and pathophysiology both inside and outside the kidney. *Physiol Rev*. 2016;96:1327–1384. doi: 10.1152/physrev.00026.2015
2. Mulatero P, Monticone S, Burrello J, Veglio F, Williams TA, Funder J. Guidelines for primary aldosteronism: uptake by primary care physicians in Europe. *J Hypertens*. 2016;34:2253–2257. doi: 10.1097/HJH.0000000000001088
3. Young WF Jr. Diagnosis and treatment of primary aldosteronism: practical clinical perspectives. *J Intern Med*. 2019;285:126–148. doi: 10.1111/joim.12831

4. Gomez-Sanchez CE, Qi X, Gomez-Sanchez EP, Sasano H, Bohlen MO, Wisgerhof M. Disordered zonal and cellular CYP11B2 enzyme expression in familial hyperaldosteronism type 3. *Mol Cell Endocrinol*. 2017;439:74–80. doi: 10.1016/j.mce.2016.10.025
5. Meyer LS, Wang X, Sušnik E, Burrello J, Burrello A, Castellano I, Eisenhofer G, Fallo F, Kline GA, Knösel T, et al. Immunohistopathology and steroid profiles associated with biochemical outcomes after adrenalectomy for unilateral primary aldosteronism. *Hypertension*. 2018;72:650–657. doi: 10.1161/HYPERTENSIONAHA.118.11465
6. Yamazaki Y, Nakamura Y, Omata K, Ise K, Tezuka Y, Ono Y, Morimoto R, Nozawa Y, Gomez-Sanchez CE, Tomlins SA, et al. Histopathological classification of cross-sectional image-negative hyperaldosteronism. *J Clin Endocrinol Metab*. 2017;102:1182–1192. doi: 10.1210/jc.2016-2986
7. Nishimoto K, Nakagawa K, Li D, Kosaka T, Oya M, Mikami S, Shibata H, Itoh H, Mitani F, Yamazaki T, et al. Adrenocortical zonation in humans under normal and pathological conditions. *J Clin Endocrinol Metab*. 2010;95:2296–2305. doi: 10.1210/jc.2009-2010
8. Boulkroun S, Samson-Couterie B, Dzib JF, Lefebvre H, Louiset E, Amar L, Plouin PF, Lalli E, Jeunemaitre X, Benecke A, et al. Adrenal cortex remodeling and functional zona glomerulosa hyperplasia in primary aldosteronism. *Hypertension*. 2010;56:885–892. doi: 10.1161/HYPERTENSIONAHA.110.158543
9. Nishimoto K, Tomlins SA, Kuick R, Cani AK, Giordano TJ, Hovelson DH, Liu CJ, Sanjanwala AR, Edwards MA, Gomez-Sanchez CE, et al. Aldosterone-stimulating somatic gene mutations are common in normal adrenal glands. *Proc Natl Acad Sci U S A*. 2015;112:E4591–E4599. doi: 10.1073/pnas.1505529112
10. Choi M, Scholl UI, Yue P, Björklund P, Zhao B, Nelson-Williams C, Ji W, Cho Y, Patel A, Men CJ, et al. K+ channel mutations in adrenal aldosterone-producing adenomas and hereditary hypertension. *Science*. 2011;331:768–772. doi: 10.1126/science.1198785
11. Oki K, Plonczynski MW, Luis Lam M, Gomez-Sanchez EP, Gomez-Sanchez CE. Potassium channel mutant KCNJ5 T158A expression in HAC-15 cells increases aldosterone synthesis. *Endocrinology*. 2012;153:1774–1782. doi: 10.1210/en.2011-1733
12. Oki K, Plonczynski MW, Lam ML, Gomez-Sanchez EP, Gomez-Sanchez CE. The potassium channel, Kir3.4 participates in angiotensin II-stimulated aldosterone production by a human adrenocortical cell line. *Endocrinology*. 2012;153:4328–4335. doi: 10.1210/en.2012-1241
13. Scholl UI, Goh G, Stölting G, de Oliveira RC, Choi M, Overton JD, Fonseca AL, Korah R, Starker LF, Kunstman JW, et al. Somatic and germline CACNA1D calcium channel mutations in aldosterone-producing adenomas and primary aldosteronism. *Nat Genet*. 2013;45:1050–1054. doi: 10.1038/ng.2695
14. Azizan EA, Poulsen H, Tuluc P, Zhou J, Clausen MV, Lieb A, Maniero C, Garg S, Bochukova EG, Zhao W, et al. Somatic mutations in ATP1A1 and CACNA1D underlie a common subtype of adrenal hypertension. *Nat Genet*. 2013;45:1055–1060. doi: 10.1038/ng.2716
15. Beuschlein F, Boulkroun S, Osswald A, Wieland T, Nielsen HN, Lichtenauer UD, Penton D, Schack VR, Amar L, Fischer E, et al. Somatic mutations in ATP1A1 and ATP2B3 lead to aldosterone-producing adenomas and secondary hypertension. *Nat Genet*. 2013;45:440–4, 444e1. doi: 10.1038/ng.2550
16. Yang Y, Gomez-Sanchez CE, Jaquin D, Aristizabal Prada ET, Meyer LS, Knösel T, Schneider H, Beuschlein F, Reincke M, Williams TA. Primary aldosteronism: KCNJ5 mutations and adrenocortical cell growth. *Hypertension*. 2019;74:809–816. doi: 10.1161/HYPERTENSIONAHA.119.13476
17. Nishimoto K, Seki T, Kurihara I, Yokota K, Omura M, Nishikawa T, Shibata H, Kosaka T, Oya M, Suematsu M, et al. Case report: nodule development from subcapsular aldosterone-producing cell clusters causes hyperaldosteronism. *J Clin Endocrinol Metab*. 2016;101:6–9. doi: 10.1210/jc.2015-3285
18. Norris JL, Caprioli RM. Analysis of tissue specimens by matrix-assisted laser desorption/ionization imaging mass spectrometry in biological and clinical research. *Chem Rev*. 2013;113:2309–2342. doi: 10.1021/cr3004295
19. Walch A, Rauser S, Deininger SO, Höfler H. MALDI imaging mass spectrometry for direct tissue analysis: a new frontier for molecular histology. *Histochem Cell Biol*. 2008;130:421–434. doi: 10.1007/s00418-008-0469-9
20. Miura D, Fujimura Y, Wariishi H. In situ metabolomic mass spectrometry imaging: recent advances and difficulties. *J Proteomics*. 2012;75:5052–5060. doi: 10.1016/j.jprot.2012.02.011
21. Ly A, Buck A, Balluff B, Sun N, Gorzolka K, Feuchtinger A, Janssen KP, Kuppen PJ, van de Velde CJ, Weirich G, et al. High-mass-resolution MALDI mass spectrometry imaging of metabolites from formalin-fixed paraffin-embedded tissue. *Nat Protoc*. 2016;11:1428–1443. doi: 10.1038/nprot.2016.081
22. Buck A, Ly A, Balluff B, Sun N, Gorzolka K, Feuchtinger A, Janssen KP, Kuppen PJ, van de Velde CJ, Weirich G, et al. High-resolution MALDI-FT-ICR MS imaging for the analysis of metabolites from formalin-fixed, paraffin-embedded clinical tissue samples. *J Pathol*. 2015;237:123–132. doi: 10.1002/path.4560
23. Sun N, Wu Y, Nanba K, Sbiera S, Kircher S, Kunzke T, Aichler M, Berezowska S, Reibetanz J, Rainey WE, et al. High-resolution tissue mass spectrometry imaging reveals a refined functional anatomy of the human adult adrenal gland. *Endocrinology*. 2018;159:1511–1524. doi: 10.1210/en.2018-00064
24. Sun N, Kunzke T, Sbiera S, Kircher S, Feuchtinger A, Aichler M, Herterich S, Ronchi CL, Weigand I, Schlegel N, et al. Prognostic relevance of steroid sulfation in adrenocortical carcinoma revealed by molecular phenotyping using high-resolution mass spectrometry imaging. *Clin Chem*. 2019;65:1276–1286. doi: 10.1373/clinchem.2019.306043 **AQ22**
25. Murakami M, Rhayem Y, Kunzke T, Sun N, Feuchtinger A, Ludwig P, Strom TM, Gomez-Sanchez C, Knosel T, Kirchner T, et al. In situ metabolomics of aldosterone-producing adenomas. *JCI Insight* 2019;4:130356. doi: 10.1172/jci.insight.130356
26. Papathomas TG, Sun N, Chortis V, Taylor AE, Arlt W, Richter S, Eisenhofer G, Ruiz-Babot G, Guasti L, Walch AK. Novel methods in adrenal research: a metabolomics approach. *Histochem Cell Biol*. 2019;151:201–216. doi: 10.1007/s00418-019-01772-w
27. Funder JW, Carey RM, Mantero F, Murad MH, Reincke M, Shibata H, Stowasser M, Young WF Jr. The management of primary aldosteronism: case detection, diagnosis, and treatment: an endocrine society clinical practice guideline. *J Clin Endocrinol Metab*. 2016;101:1889–1916. doi: 10.1210/jc.2015-4061
28. Williams TA, Reincke M. MANAGEMENT OF ENDOCRINE DISEASE: Diagnosis and management of primary aldosteronism: the Endocrine Society guideline 2016 revisited. *Eur J Endocrinol*. 2018;179:R19–R29. doi: 10.1530/EJE-17-0990
29. Sun N, Ly A, Meding S, Witting M, Hauck SM, Ueffing M, Schmitt-Kopplin P, Aichler M, Walch A. High-resolution metabolite imaging of light and dark treated retina using MALDI-FTICR mass spectrometry. *Proteomics*. 2014;14:913–923. doi: 10.1002/pmic.201300407
30. Mantini D, Petrucci F, Pieragostino D, Del Boccio P, Di Nicola M, Di Ilio C, Federici G, Sacchetta P, Comani S, Urbani A. LIMPIC: a computational method for the separation of protein MALDI-TOF-MS signals from noise. *BMC Bioinformatics*. 2007;8:101. doi: 10.1186/1471-2105-8-101
31. Wishart DS, Feunang YD, Marcu A, Guo AC, Liang K, Vázquez-Fresno R, Sajed T, Johnson D, Li C, Karu N, et al. HMDB 4.0: the human metabolome database for 2018. *Nucleic Acids Res*. 2018;46:D608–D617. doi: 10.1093/nar/gkx1089
32. Palmer A, Phapale P, Chernyavsky I, Lavigne R, Fay D, Tarasov A, Kovalev V, Fuchser J, Nikolenko S, Pineau C, et al. FDR-controlled metabolite annotation for high-resolution imaging mass spectrometry. *Nat Methods*. 2017;14:57–60. doi: 10.1038/nmeth.4072
33. Chong J, Soufan O, Li C, Caraus I, Li S, Bourque G, Wishart DS, Xia J. MetaboAnalyst 4.0: towards more transparent and integrative metabolomics analysis. *Nucleic Acids Res*. 2018;46:W486–W494. doi: 10.1093/nar/gky310
34. Xia J, Wishart DS. MetPA: a web-based metabolomics tool for pathway analysis and visualization. *Bioinformatics*. 2010;26:2342–2344. doi: 10.1093/bioinformatics/btq418
35. Kanehisa M, Goto S. KEGG: Kyoto Encyclopedia of Genes and Genomes. *Nucleic Acids Res*. 2000;28:27–30. doi: 10.1093/nar/28.1.27
36. Yang Y, Burrello J, Burrello A, Eisenhofer G, Peitzsch M, Tetti M, Knösel T, Beuschlein F, Lenders JWM, Mulatero P, et al. Classification of microadenomas in patients with primary aldosteronism by steroid profiling. *J Steroid Biochem Mol Biol*. 2019;189:274–282. doi: 10.1016/j.jsbmb.2019.01.008
37. Sugiura Y, Takeo E, Shimma S, Yokota M, Higashi T, Seki T, Mizuno Y, Oya M, Kosaka T, Omura M, et al. Aldosterone and 18-oxocortisol coaccumulation in aldosterone-producing lesions. *Hypertension*. 2018;72:1345–1354. doi: 10.1161/HYPERTENSIONAHA.118.11243
38. Buck A, Heijs B, Beine B, Schepers J, Cassese A, Heeren RMA, McDonnell LA, Henkel C, Walch A, Balluff B. Round robin study of formalin-fixed paraffin-embedded tissues in mass spectrometry imaging.

Anal Bioanal Chem. 2018;410:5969–5980. doi: 10.1007/s00216-018-1216-2

39. Schwartz L, Supuran CT, Alfarouk KO. The warburg effect and the hallmarks of cancer. *Anticancer Agents Med Chem*. 2017;17:164–170. doi: 10.2174/1871520616666161031143301
40. Nacarelli T, Lau L, Fukumoto T, Zundell J, Fatkhutdinov N, Wu S, Aird KM, Iwasaki O, Kossenkov AV, Schultz D, et al. NAD+ metabolism governs the proinflammatory senescence-associated secretome. *Nat Cell Biol*. 2019;21:397–407. doi: 10.1038/s41556-019-0287-4
41. Otis M, Campbell S, Payet MD, Gallo-Payet N. Expression of extracellular matrix proteins and integrins in rat adrenal gland: importance for ACTH-associated functions. *J Endocrinol*. 2007;193:331–347. doi: 10.1677/JOE-07-0055
42. Swierczynska MM, Betz MJ, Colombi M, Dazert E, Jenö P, Moes S, Pfaff C, Glatz K, Reincke M, Beuschlein F, et al. Proteomic landscape of aldosterone-producing adenoma. *Hypertension*. 2019;73:469–480. doi: 10.1161/HYPERTENSIONAHA.118.11733
43. Williams TA, Jaquin D, Burrello J, Philippe A, Yang Y, Rank P, Nirschl N, Sturm L, Hübener C, Dragun D, et al. Diverse responses of autoantibodies to the angiotensin II type 1 receptor in primary aldosteronism. *Hypertension*. 2019;74:784–792. doi: 10.1161/HYPERTENSIONAHA.119.13156
44. Armanini D, Sabbadin C, Bordin L. Enigma of the origin of primary aldosteronism. *Hypertension*. 2019;74:745–746. doi: 10.1161/HYPERTENSIONAHA.119.13302
45. Burrello J, Burrello A, Stowasser M, Nishikawa T, Quinkler M, Prejbisz A, Lenders JWM, Satoh F, Mulatero P, Reincke M, et al. The primary aldosteronism surgical outcome score for the prediction of clinical outcomes after adrenalectomy for unilateral primary aldosteronism. *Ann Surg*. doi: 10.1097/SLA.0000000000003200 [Epub ahead of print]. AQ23

Novelty and Significance

What Is New?

- We performed in situ metabolic mass spectrometry imaging (mass resolution matrix-assisted laser desorption/ionization Fourier-transform ion cyclotron resonance mass spectrometry imaging) of selected cell populations of formalin-fixed paraffin-embedded adrenals from patients with primary aldosteronism.
- Specific distribution patterns of metabolites were associated with aldosterone-producing cell clusters (APCCs) and identified 2 specific subgroups of APCCs (subgroups 1 and 2).

What Is Relevant?

- The metabolic profiles of APCCs in subgroup 1 were tightly clustered and clearly distinct from those of subgroup 2 and aldosterone-producing adenomas.
- The metabolic profiles of APCCs in subgroup 2 were highly similar to those of aldosterone-producing adenomas.
- Metabolic pathways that support cell proliferation were enhanced in APCC subgroup 2 compared with subgroup 1.

Summary

We applied high mass resolution matrix-assisted laser desorption/ionization mass spectrometry imaging to formalin-fixed paraffin-embedded adrenals from patients with unilateral PA and provide evidence from metabolic phenotyping and pathway analyses that a subset of APCCs may transition to aldosterone-producing adenomas.